ACS SENSORS

pubs.acs.org/acssensors
Article

Rational Approach to Optimizing Conformation-Switching Aptamers for Biosensing Applications

Monica Wolfe, Alyssa Cramer, Sean Webb, Eva Goorskey, Yaroslav Chushak, Peter Mirau, Netzahualcóyotl Arroyo-Currás, and Jorge L. Chávez*

Cite This: ACS Sens. 2024, 9, 717–725
Read Online

ACCESS | Metrics & More | Article Recommendations | Supporting Information

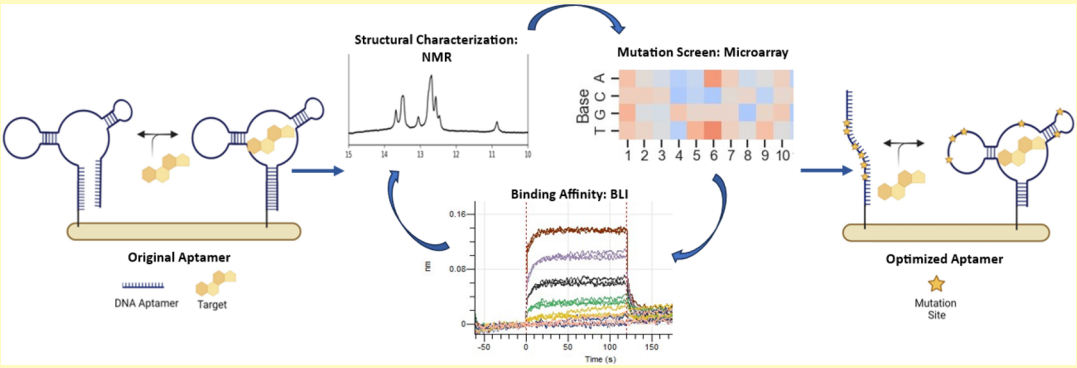

ABSTRACT: The utilization of structure-switching aptamers (SSAs) has enabled the development of novel sensing platforms for the sensitive and continuous detection of molecules. *De novo* development of SSAs, however, is complex and laborious. Here we describe a rational approach to SSA optimization that simultaneously improves aptamer binding affinity and introduces target-dependent conformation-switching for compatibility with real-world biosensor applications. Key structural features identified from NMR and computational modeling were used to optimize conformational switching in the presence of target, while large-scale, microarray-based mutation analysis was used to map regions of the aptamer permissive to mutation and identify combinations of mutations with stronger binding affinity. Optimizations were carried out in a relevant biofluid to ensure a seamless transition of the aptamer to a biosensing platform. Initial proof-of-concept for this approach is demonstrated with a cortisol binding aptamer but can easily be translated to other relevant aptamers. Cortisol is a hormone correlated with the stress response that has been associated with various medical conditions and is present at quantifiable levels in accessible biofluids. The ability to continuously track levels of stress in real-time via cortisol monitoring, which can be enabled by the aptamers reported here, is crucial for assessing human health and performance.

KEYWORDS: *cortisol, stress, aptamers, sequence optimization, microarray, structure-switching, biosensors, NMR*

The design of rapid, continuous, reagentless, and noninvasive sensors remains a fundamental challenge for the biosensing community due to the high sensitivity and specificity required for sensing in biofluids. To achieve this type of sensing, it is important that the biorecognition element of the sensing platform has certain characteristics, such as rapid and reversible binding; criteria that preclude the use of most antibodies and antibody-like receptors. Alternatively, structure-switching aptamers (SSA) have the ability to undergo a conformational change in the presence of their target molecule. The switch between the nonbinding and binding conformations is controlled by both the stability of the aptamer structure (ΔG) and the affinity of the target for the sequence (K_D).[1] Although both aptamer conformations exist in equilibrium, the presence of the target stabilizes the binding state and reinforces aptamer structure.[2] For sensing, this conformational change can be leveraged to transduce fluorescence, colorimetric, and electrochemical signals for incorporation into various biosensor platform formats.[3−7]

While the field of SSA research has grown significantly over the past decade,[8] the process of converting a traditional aptamer into an SSA postselection remains challenging and relies largely on trial and error.[1] A recent advance in this area has led to the development of a high-throughput screening platform that can convert traditional aptamers into SSAs.

Received: September 22, 2023
Revised: December 1, 2023
Accepted: January 10, 2024
Published: January 25, 2024

However, this approach relies on the presence of a complementary displacement strand to achieve switching behavior.[9] Strategies to directly select for structure switching aptamers (e.g., capture-SELEX) have similar limitations,[10−12] which restrict sensing to single use applications unless laborious aptamer truncations are performed to optimize conformation-based signaling. Furthermore, aptamer structure and function are often explicitly linked to the buffer conditions used during selection, rendering some aptamers nonfunctional in the more complex environment of biofluids.

In response to these limitations, we sought to establish a robust and rational aptamer optimization strategy that introduces reporter-independent conformation-switching capability and improves target affinity in biofluids relevant to continuous sensing applications. Our approach includes structural characterization at the molecular level using NMR and computer modeling to identify sequence-specific binding features and conformations. NMR also allows us to visualize aptamer conformational changes in the presence and absence of a target, thereby streamlining the optimization of switching behavior required for sensing applications. In parallel, we also perform a strand-displacement-based large-scale mutational analysis using a microarray-based platform. This allows for the simultaneous assessment of all possible aptamer point mutations and rapid screening of combinatorial mutations for improved binding affinity. Finally, all binding affinity characterization of aptamer sequences was performed using Bio-Layer Interferometry (BLI), immobilizing the sequences as a single stranded DNA with no additional labels or complementary sequence needed, mimicking potential use in sensing platforms. Because translation of these results to real world sensing environments is critical for success, we performed all work in a biologically relevant buffer and further showed that our optimized sequence performed well in human biofluid.

As a proof of concept for this approach, we initially focused on cortisol as a model system. Continuous, real-time monitoring of stress hormones is in demand for the prevention of negative performance outcomes and the diagnosis and management of disease.[13] Cortisol, a small molecule steroid hormone, plays an important role in the stress-responsive hypothalamus-pituitary-adrenal (HPA) axis and is involved in a range of bodily processes, including proteolysis, glucose regulation, blood pressure, and immune responses.[14] Cortisol dysregulation occurs in a number of conditions and has been linked to fatigue, obesity, post-traumatic stress disorder, anxiety disorders, depression, and poor performance.[15] Cortisol is present at nanomolar concentrations in blood and recent clinical studies have shown a correlation between cortisol levels in blood and other bodily fluids such as sweat, saliva, urine, and interstitial fluid (ISF).[16−19] ISF, in particular, is attractive for biosensing because it has a composition similar to blood plasma but, unlike blood, can be drawn continuously from the dermis using noninvasive and compliance-free methods.[20] Recently, electrochemical aptamer-based (EAB) sensing on microneedles was validated for continuous *in vivo* measurement of molecules in ISF.[21−23] The ability to track cortisol and other stress hormones in real-time should be advantageous for the assessment of overall physiological health and performance. While this work focuses on the structural characterization and optimization of a cortisol binding aptamer, we believe this approach can be broadly applied to optimize SSAs for other relevant targets and support the development of real-time, continuous biomarker sensors.

EXPERIMENTAL SECTION

Materials. Oligonucleotide sequences were synthesized and HPLC purified by Integrated DNA Technologies (Coralville, Iowa). All oligonucleotides were dissolved in nuclease-free water at 100 μM and stored at −20 °C. Unless noted otherwise, all chemicals and reagents were purchased from Sigma-Aldrich (St. Louis, MO). Target compounds were solubilized in DMSO (Sigma-Aldrich, St. Louis, MO) at a stock concentration of 10 mM. Experiments were performed in phosphate buffered saline (PBS), binding buffer (50 mM Tris-HCl, 300 mM NaCl, 5 mM MgCl, 30 mM KCl, pH 7.4), simulated ISF (sISF, recipe in Supporting Information S1), or pooled human serum (Innovative Research, Novi, MI).

Nuclear Magnetic Resonance (NMR). NMR spectra for the aptamer and aptamer-cortisol complexes were obtained at 400, 600, and 800 MHz on Bruker and Tecmag NMR spectrometers. The samples were prepared in sISF containing 10% D_2O for NMR locking. The imino proton spectra were observed using the excitation sculpting pulse sequence with a 2 ms water inversion pulse.[24] A concentrated cortisol stock solution was prepared in DMSO-d6 and 5 uL was added to the NMR sample to give the 1:1 complex. The concentration of DNA aptamer was 1.0 mM. Experiments were performed at 25 °C. The 2D Nuclear Overhauser Spectroscopy (NOESY) spectra were measured in PBS containing 10% D_2O at 800 MHz and 283 K with a 200 ms mixing time.[25]

***In Silico* Modeling.** The secondary structure and folding energy of the cortisol-binding aptamers were calculated using the UNAFold web server[26] with inputs of 300 mM NaCl, 5 mM Mg^{2+} and 25 °C for consistency with initial selection buffer conditions. The 3D structures of the ssDNA aptamers were generated in two steps. Initially, thousands of tertiary structure models for the equivalent ssRNA sequence were produced using the RNA *de novo* protocol through Fragment Assembly of RNA with Full Atom Refinement (FARFAR) from the Rosetta package.[27] Five models with the lowest energy and with the presence of a noncanonical GA base pair (see NMR results) were selected for the second step to evaluate their stability using Molecular Dynamics simulations. The selected ssRNA structures were converted into ssDNA models by transforming the uracil residues to thymine and replacing the ribose sugar backbone with deoxyribose using the LEaP program of the Amber20 suite of biomolecular simulation programs.[28] The obtained DNA molecules were solvated with TIP3P water in a rectangular box with periodic boundary conditions. Na^+ and Cl^- ions were added to maintain the neutrality of the system and the experimental salt concentration. Initially, system was equilibrated at ambient conditions with fixed backbones for 300 ps using the sander program of the Amber20 package. Second, the whole system was equilibrated for 300 ps and, finally, the production run was performed for 2 ns. During the production run 100 conformations were saved for stability analysis. The stability of ssDNA structures was determined based on the variability of configurational energy and GA base pair distance. Five conformations of the most stable structure separated by 200 ps of simulations were selected for modeling of cortisol binding. The docking of cortisol to the DNA aptamer was performed using the PatchDock web server developed based on shape complementary principles.[29] Both cortisol and aptamer were considered rigid, and a global search of the rotational and translational space was performed without any constraints on the locations of the binding site. Two cortisol-aptamer complexes with the highest scoring were selected for each of the DNA conformations and analyzed to identify the cortisol-binding site. The visualization of molecules was performed using the UCSF Chimera package.[30]

Bio-Layer Interferometry (BLI). BLI was used to determine equilibrium dissociation constants (K_D) for each aptamer to target molecule. Experiments were performed in binding buffer or sISF at 30 °C. Aptamer sequences were synthesized with a 5′ biotin tag (Integrated DNA Technologies, Coralville, Iowa) and immobilized onto SuperStreptavidin biosensor tips (Sartorious, Gottingen, Germany) for binding affinity characterization on the Octet Red96e (Sartorious, Gottingen, Germany). Briefly, aptamer-loaded tips were

https://doi.org/10.1021/acssensors.3c02004
ACS Sens. 2024, 9, 717−725

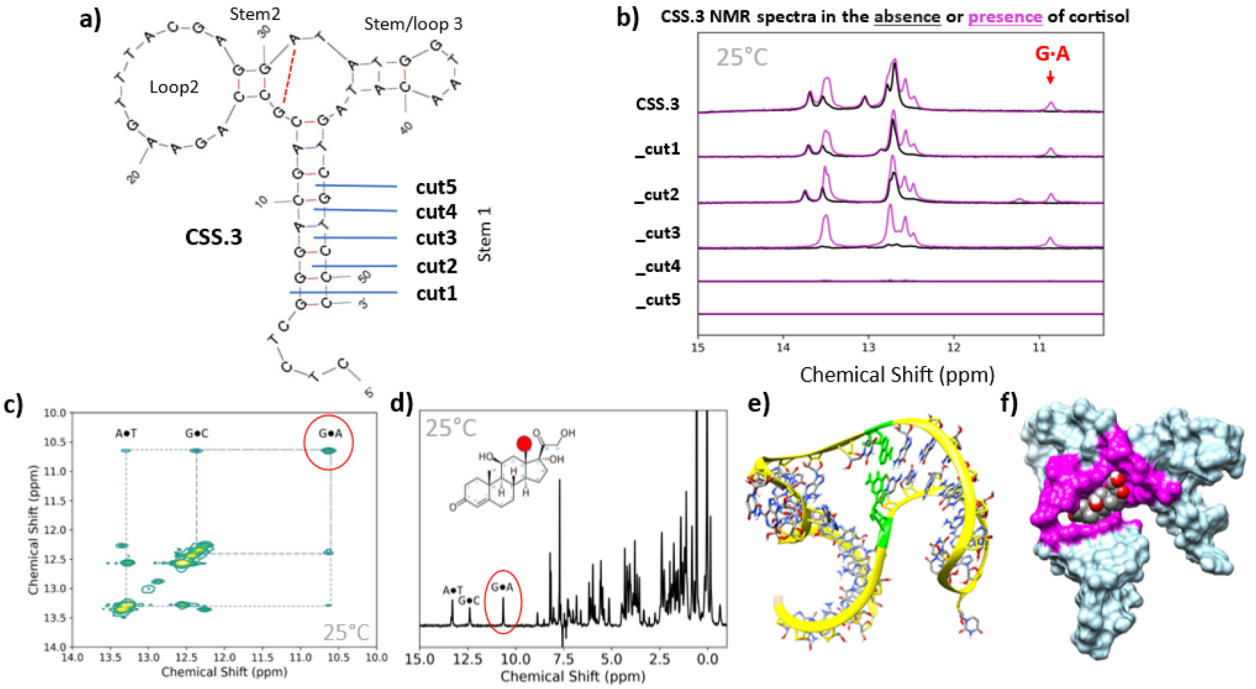

Figure 1. Structural Characterization of CSS.3 aptamer and stem truncations. (a) MFold-Predicted Secondary Structure of CSS.3 showing location of cut sites for Stem #1 truncation. (b) NMR spectra of aptamer variants in the absence (black) or presence (magenta) of cortisol show loss of structure with stem truncation. Additional peaks, including a noncanonical GA base pair, form in the presence of cortisol (10.9 ppm). CSS.3_cut3 appears to be unstructured in solution but still retains the ability to bind cortisol. (c) 800 MHz 2D NOESY NMR spectra of CSS.3_cut3 in the presence of cortisol and (d) a cross section through the 2D NOESY spectrum showing magnetization exchange from the cortisol methyl protons both show the interaction of the GA base pair with cortisol. (e) Rigid 3D structure of CSS.3_cut3 in its binding conformation with predicted noncanonical GA base pair highlighted in green. (f) 3D model of CSS.3_cut3 aptamer docked to cortisol with binding pocket highlighted in magenta. All experiments were conducted in sISF containing 10% D_2O at 25 °C.

baselined in the experimental buffer for 30 s before binding. An additional 180 s pre-equilibration step was added following aptamer loading for experiments run in sISF to allow for a stable signal prior to baseline. Association and dissociation steps were both 120 s long (binding buffer or sISF). Data were double reference subtracted using a buffer only control well and scrambled aptamer sequence. Due to the rapid kinetics of small molecule binding, dissociation constants (K_D) were calculated using steady state curve fitting from the average of three replicate runs (one-site specific binding; GraphPad Prism v9.3).

Microarray. Custom DNA microarrays were synthesized by Agilent Technologies (Santa Clara, CA). Sequences were printed onto the glass surface starting at the 3′ end and linked by a variable length T spacer such that all sequences were 60 nucleotides in length. A minimum of 3 replicates were printed for each sequence. Control sequences were also included for the array validation and grid fitting. Prior to screening, microarray slides were rehydrated in a water bath (42 °C) for 30 min. Using an Agilent hybridization chamber (including base, cover, and clamp assembly) and backing slide, sub arrays were coincubated for 1 h with fluorescently labeled capture probe (100 μM Probe-Cy5; 5′-GTCGTCCCGAGAGCCATA-Cy5−3′) and cortisol (0−300 μM). Counter targets were screened at equimolar concentrations of 300 μM unless otherwise indicated. All experiments were performed in sISF + BSA. A control array (100 μM Probe-Cy5 only) was included on each slide and used to establish the baseline fluorescence for data analysis. After hybridization, slides were washed by dipping for 10 s in binding buffer, then PBS. To remove any residual buffer salts before imaging, slides were quickly dipped in nuclease-free water and dried under a stream of nitrogen. Slides were imaged on a fluorescent scanner (Agilent SureScan Microarray Scanner) at a wavelength of 635 nm (red channel) with 3 um resolution and a 20-bit dynamic range. Median background-subtracted spot intensities were extracted from each spot using Mapix Analysis software (v1.8, Innopsys) and normalized to compare probe hybridization across all subarrays (eq 1).

$$\text{probe hybridization}(\%\text{Max}) = \frac{(x - \text{Min})}{(\text{Max} - \text{Min})} \quad (1)$$

where x represents the raw fluorescence intensity for a particular spot and Min and Max represent mean fluorescence intensity for positive and negative probe hybridization control spots, respectively. Target-induced probe dissociation was then calculated as %Change (eq 2) relative to a blank (probe only) control array.

$$\text{probe dissociation}(\%\text{Change}) = \%\text{Max}_{\text{blank}} - \%\text{Max}_{\text{target}} \quad (2)$$

Data in graphs represent the mean ± standard deviation (SD) for all replicates of a given sequence.

RESULTS AND DISCUSSION

Aptamer Structural Characterization and Switching. For this work we consider a cortisol binding aptamer discovered by Yang et al. using a strand displacement SELEX technique.[31] The aptamer, named CSS.3, was one of three cortisol aptamers reported by Yang et al., but it demonstrated the highest affinity compared to the other two sequences. Our own internal work confirmed that CSS.3 had the best binding affinity in binding buffer with a K_D of 240 nM (Supporting Information S2). Structurally, CSS.3 is predicted to form a three-way junction motif consisting of a central loop flanked by three stem regions (MFold predicted structure shown in Figure 1a). Although originally selected using a strand displacement technique common for the identification of structure switching aptamers, through extensive literature research we could not find experimental data demonstrating

https://doi.org/10.1021/acssensors.3c02004
ACS Sens. 2024, 9, 717−725

a)

Aptamer	K_D +/- SD (nM) Cortisol in sISF	R^2
CSS.3	660 +/- 33	0.99
_cut1	530 +/- 23	0.99
_cut2	560 +/- 40	0.98
_cut3	990 +/- 59	0.98
_cut4	1300 +/- 69	0.99
_cut5	4200 +/- 99	0.99

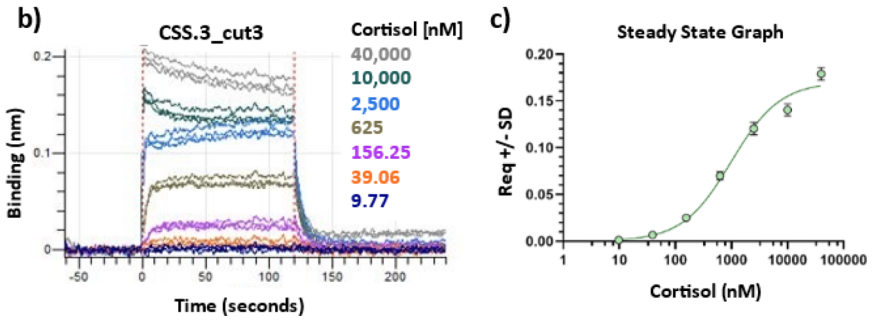

Figure 2. Binding for all CSS.3 aptamer truncations was measured by using BLI. (a) Calculated binding affinities from steady state equilibrium to cortisol in sISF. (b) Replicate traces showing real-time baseline, association and dissociation and (c) averaged steady state binding traces for stem-optimized CSS.3_cut3 aptamer are featured. SD = standard deviation. Experiments were conducted at 30 °C in sISF.

the aptamer is structure switching nor structural characterization data. A report by Niu et al. characterized binding affinity of CSS.1 (one of the other cortisol aptamers reported by Yang et al.) and various CSS.1 truncations, however, the authors did not perform any structural characterizations of the aptamer.[32]

Using NMR to characterize aptamer structure, we show here that the CSS.3 aptamer has peaks in the 13−14 and 12−13 ppm range (Figure 1b, top line, black trace), corresponding to AT and GC base pairs, respectively.[33,34] The addition of cortisol results in the appearance of new peaks, most notably a distinct peak appearing at 10.9 ppm (Figure 1b, top line, magenta trace). Based on the mfold predicted structures and previous NMR studies on noncanonical base pairs[35−37] we propose that this new peak is due to the formation of a GA base pair forming in the central loop region adjacent to stem 2 (denoted by dotted red line in Figure 1a). Because it is formed only in the presence of cortisol, we propose that the cortisol binding site is partially formed by this GA base pair. This is a notable finding because the presence of a noncanonical base pair forming within the binding pocket cannot be predicted using modeling software alone. Cortisol binding is also confirmed by large chemical shifts for the cortisol methyl protons in the aliphatic portion of the CSS.3 NMR spectra (Supporting Information S3).

Based on this structural characterization work, we concluded that the CSS.3 aptamer is mostly folded in the absence of cortisol and would be unlikely to undergo a sufficiently large conformational switch for signal generation without the addition of a displacement strand. Recently, a wearable cortisol sweat sensor was developed using the CSS.3 sequence, however, in line with our findings here, the aptamer was modified into a pseudoknot structure to assist with conformation-switching for electrochemical signal generation.[38] We hypothesized that because the aptamer was selected using a strand displacement technique,[31] further optimization would be needed in order to engineer a robust conformational change without the presence of a complementary displacement strand.

Aptamer Truncations Effects on Structure Switching. To introduce structure switching, we systematically examined the effect of truncating the stem no. 1 region of the aptamer, as depicted by the cuts shown in Figure 1a (sequences provided in Supporting Information S4). Based on similar rational design approaches,[39−42] we expected there to be an increase in structure-switching capability but a loss of binding affinity as the length of the stem region was reduced. However, it was unclear from the computationally derived data at what point the optimal balance for switching would occur. To assess structure switching in the truncated aptamers, we looked at the aptamer structure in the presence and absence of cortisol using NMR. Figure 1b shows the spectra for all CSS.3-truncated aptamers in the absence (black) and presence (magenta) of cortisol. With each sequential aptamer truncation there is a loss of structure, as evidenced by the loss of peaks in the 12−14 ppm region. With the removal of three base pairs (cut3) the aptamer no longer shows any discernible peaks in this region, which is consistent with the aptamer being unstructured in solution. Notably, once exposed to cortisol, this truncation still retains the ability to bind cortisol, as evidenced by the presence of peaks in the 12−14 ppm region and the GA base pair indicated by the peak at 10.9 ppm. No imino or upfield proton peaks are observed for CSS.3_cut4 or _cut5 in either spectrum, indicating that these sequences remain unstructured even in the presence of cortisol. From the NMR spectra, we selected CSS.3_cut3 as the optimal truncation for maximal structure switching in response to cortisol binding.

In addition to this work, we also performed 2D NOESY NMR analysis on the stem-optimized CSS.3_cut3 aptamer, with the goal of identifying the cortisol binding site. The spectra in Figure 1c was acquired in PBS (we found little difference between DNA duplexes tested in PBS vs sISF, Supporting Information S5) and at a lower temperature (283 K) to decrease the water exchange rate with a long mixing time (200 ms) so that protons separated by longer distances, including those between neighboring imino protons.[25] Figure 1d shows a cross section of the NOESY spectra. These data show numerous exchange peaks that arise both from inter and intramolecular magnetization exchange. Of particular interest are the cross peaks to the imino protons from the GC and AT base pairs, as well as the GA base pair within the central loop. These data confirm that cortisol binds within the central loop of the three-way junction structure and is in close proximity to the GA base pair.

Furthermore, we used the structural insights gained from NMR to model the docking of the CSS.3_cut3 aptamer to cortisol. Because no reliable tools exist for rigid 3D ssDNA modeling, we generated the initial structure using RNA modeling software and then converted it into DNA before subjecting it to molecular dynamics simulations (see the Experimental Section for details). Importantly, when selecting structures, we looked for models where the GA base pair in the central region would be likely to form due to the proximity of the two nucleotides. This process generated a rigid 3D

https://doi.org/10.1021/acssensors.3c02004
ACS Sens. 2024, 9, 717−725

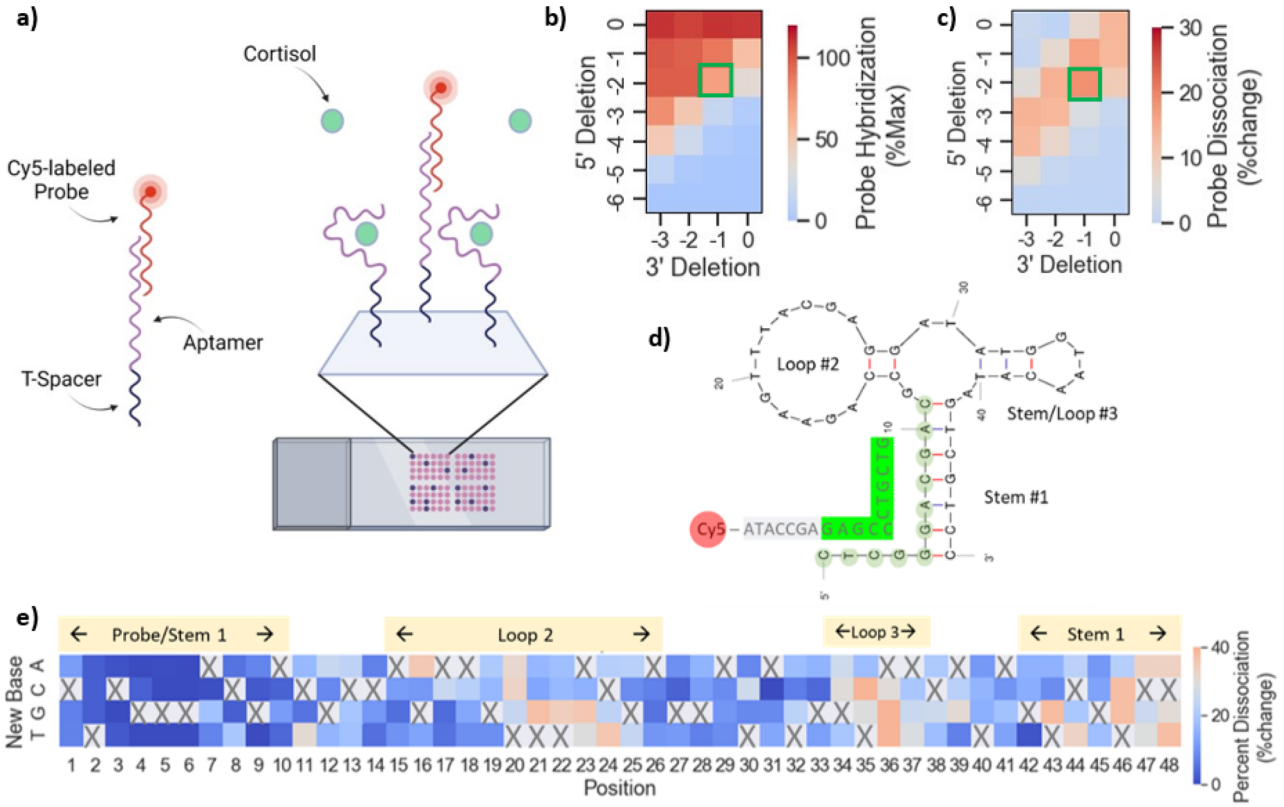

Figure 3. Microarray-based target-induced probe dissociation screening. (a) Schematic showing probe dissociation strategy with a fluorescently labeled probe designed to hybridize to the 5′ region of the aptamer and dissociate in the presence of cortisol. (b) Optimization of stem #1 length for probe hybridization and (c) cortisol-induced probe dissociation signal. (d) The optimized CSS.3 sequence (5′del2, 3′del1) and fluorescently labeled probe is shown with complementary region highlighted in green. (e) Heatmap showing cortisol-induced probe dissociation for all possible point mutations of the CSS.3 parent sequence and identifies two regions permissible to mutation. Mutation introduced is shown along the *y*-axis and position along the aptamer on *x*-axis. Probe dissociation was color-coded such that red/orange = improved binding; blue = worsened binding; gray = no change relative to parent sequence (threshold = 29%). Microarray experiments were conducted at room temperature, in sISF + BSA.

structure of CSS.3_cut3 (Figure 1e, with the GA base pair highlighted in green), which was docked to cortisol. The 3D docked model shows binding occurring within the central loop of the aptamer and with extensive interactions between base pairs in stems 1 and 3, as well as the GA base pair (Figure 1f, interacting nucleotides highlighted in magenta). We postulate that advances in ssDNA modeling will enable more robust sequence optimization efforts in the future.

Sequence Optimization for Improved Affinity. While a robust conformational change is important for sensor integration, it is also important to maintain a high binding affinity between the aptamer and target. Here we used BLI to measure the binding affinity for each of the CSS.3 aptamer variants in sISF. The measured binding affinities for each of the aptamer truncations are shown in Figure 2a. CSS.3_cut3 shows some loss of cortisol binding affinity with a K_D of 990 nM compared with 660 nM for the full-length aptamer. CSS.3_cut1 and CSS.3_cut2 show slight improvement in binding affinity, likely due to easier folding with the removal of nonessential nucleotides from the 3′ end. Removal of more than three base pairs from the stem #1 region results in more significant loss of binding affinity; the K_D value for cut 5 was found to be 4200 nM. These findings are consistent with the NMR findings in that removal of more than three bases from the stem region results in destabilization of the aptamer structure, such that cortisol binding affinity is negatively affected. We believe the BLI technique allows us to quantify weaker interactions that we are allowed to measure in the NMR experiments, which would explain the difference observed in the data shown in Figure 1b (no binding observable by NMR for the sequences labeled cut 4 and 5) while a measurable K_D is observed by BLI (Figure 2a). The overlaid traces in Figure 2b,c show real-time baseline, association, and dissociation to cortisol and steady state curve fitting results for CSS.3_cut3.

The results from the binding affinity determination highlight another important finding. When tested in sISF, a more biologically relevant and complex buffer, the CSS.3 aptamer undergoes an almost 3-fold loss of affinity (the K_D for CSS.3 dropped from 249 nM in tris binding buffer (Supporting Information S2) to 660 nM in sISF (Figure 2a). Given the combined deleterious effects of both stem truncation and biofluid composition on binding affinity, we sought to further improve the aptamer performance for real world sensing applications.

Microarray-Based Sequence Maturation Screening. We carried out large-scale sequence maturation and screening experiments using microarrays, with the goal of identifying better binders in sISF. Because cortisol is a small molecule and therefore has a limited number of epitopes available for binding, we used a strand-displacement approach for microarray screening (Figure 3a). Like strand-displacement SELEX, we used a displacement probe with a fluorescent label as an indirect measure of cortisol binding. In the absence of cortisol,

https://doi.org/10.1021/acssensors.3c02004
ACS Sens. 2024, 9, 717−725

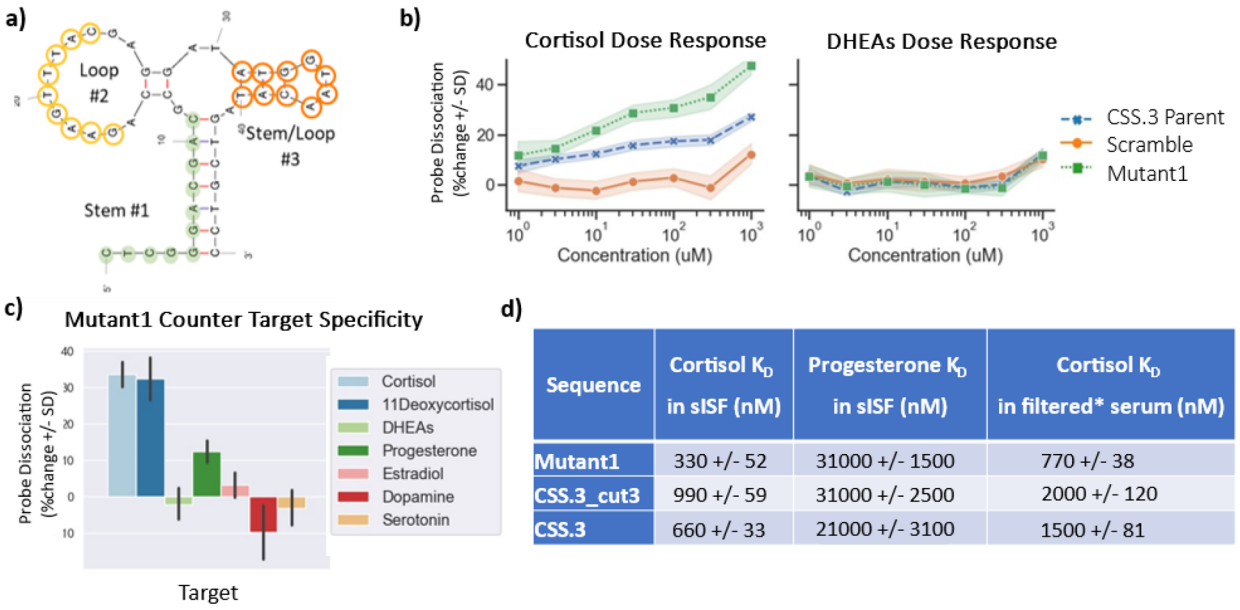

Sequence	Cortisol K_D in sISF (nM)	Progesterone K_D in sISF (nM)	Cortisol K_D in filtered* serum (nM)
Mutant1	330 +/- 52	31000 +/- 1500	770 +/- 38
CSS.3_cut3	990 +/- 59	31000 +/- 2500	2000 +/- 120
CSS.3	660 +/- 33	21000 +/- 3100	1500 +/- 81

Figure 4. Sequence optimization of the CSS.3 aptamer for an improved binding affinity. (a) Regions selected for nucleotide randomization in loop #2 (yellow) and stem and loop #3 (orange) are highlighted. (b) Dose−response curves showing increased probe dissociation for mutant compared to CSS.3 parent sequence and scrambled negative control sequence in the presence of cortisol (left) but not DHEAs (right). (c) Specificity of optimized mutant showing strong response to cortisol and 11-deoxycortisol, moderate response to progesterone and no response to other structurally similar targets. (d) DNA sequences were immobilized on BLI sensor tips through biotin and binding to cortisol was measured directly (without the use of complementary sequences), it is demonstrated that the selected mutant has 3-fold better binding affinity and selectivity against progesterone compared to the stem-optimized CSS.3_cut3 sequence. The mutant sequence also performs better in filtered human serum as a surrogate for testing in real ISF. (*) Serum filtered using 30 kDa MWCO filter.

the probe hybridizes to complementary bases on the 5′ end of the aptamer and forms a duplex. Upon binding to cortisol, the aptamer undergoes a conformational change that displaces the probe. Unbound probe is then removed during the washing step. The amount of probe dissociation in the presence of cortisol can be calculated relative to a buffer control and is used to estimate binding. A similar microarray-based approach has been used previously for aptamer optimization,[43] but differed in that the probe hybridized to the target binding site and competed directly with the target for binding.

Probe Hybridization Optimization. For this approach to be successful, it is important to first optimize the kinetics of probe hybridization. If probe hybridization is too strong, then it can prevent the transition of the aptamer into its binding conformation. Conversely, if probe hybridization is too weak, it is likely to dissociate even in the absence of target.[1] To achieve measurable binding signal for the CSS.3 aptamer, we first studied the effect of 5′ and 3′ truncations on probe hybridization and cortisol-induced probe dissociation (Figure 3b,c). The full-length CSS.3 parent sequence is represented by the square in the upper right corner of the heatmaps (5′del0, 3′del0), and combinations of both 5′ and 3′ truncations can be mapped by moving down and left, respectively, across the heatmap. Regarding probe hybridization (Figure 3b), we found that hybridization weakened as nucleotides were deleted from the 5′ region of the aptamer. This was expected, since the 5′ region is complementary to the probe, and removal of nucleotides from that region would be expected to weaken probe hybridization. Conversely, as nucleotides were deleted from the 3′ region of the aptamer, probe hybridization strengthened because aptamer folding became weaker with fewer base pairs present in stem #1, therefore making it easier for the probe to hybridize. Regarding cortisol-induced dissociation (Figure 3c), we found an inverse relationship to that of probe hybridization. As bases were removed from the 5′ region of the aptamer, cortisol binding increased. Again, this result was expected, because probe hybridization would be weakened and easier to displace upon binding. Similarly, cortisol-induced probe dissociation decreased with the removal of bases from the 3′ region. We believe this is due to the weakening of stem #1, therefore making it harder for the aptamer to fold into its binding conformation and displace the probe. Sequences at the bottom right corner of the heatmap showed no cortisol-induced probe dissociation due to the lack of initial probe hybridization.

The sequences with measurable cortisol binding can be visualized as a diagonal band across the heatmap in Figure 3c. For microarray screening, we chose the sequence shown in Figure 3d (5′del2, 3′del1; boxed in green in Figure 3b,c) as the optimized parent sequence for microarray screening. Although probe hybridization was slightly lower with this truncation than that for the full-length CSS.3 aptamer, it showed high sensitivity to cortisol.

Mapping Aptamer Sequence Space Amenable to Mutations. For sequence optimization, we first focused on identifying regions of the aptamer that are amenable to mutation. We anticipated that residues close to the binding pocket would have the highest impact on the binding affinity; thus, it was unclear which positions could be mutated without disrupting cortisol binding. Using the microarray, we looked at the cortisol responses for all possible single point mutants of the CSS.3 parent aptamer (Figure 3e). Probe dissociation in the heatmap is color-coded such that blue is nonbinding, orange is improved binding, and gray is no change from parent sequence (%change of CSS.3 parent = 29%). The data show that most positions could not be mutated without negatively

https://doi.org/10.1021/acssensors.3c02004
ACS Sens. 2024, 9, 717−725

affecting cortisol binding. This included mutation of positions 12 and 29; the nucleotides involved in the GA base pair identified from NMR structural characterization. The only regions permissive to mutation were nucleotides 16, 20−24 and 34−37, which correspond to the outer part of loop #2 and loop #3.

While the microarray point mutation findings were largely consistent with the binding pocket identified from NMR, they also highlight the importance of residues not otherwise identified. For example, single point mutations in regions of loop #2 (e.g., positions 17−19) also resulted in loss of binding. These residues were not highlighted as binding sites by either NMR nor structural modeling and would not be expected to be important from a rational design approach, since unpaired bases in loop #2 would be least likely to be involved in stabilizing aptamer binding conformation or interacting directly with cortisol. Similar to other aptamer optimization efforts,[9,44] these findings further highlight the importance of large-scale mutational analysis in sequence optimization approaches. While this work focuses on the optimization of a cortisol binding aptamer, we have also had success in applying this approach to aptamers for other targets such as DHEAs (Supporting Information S6).

Aptamer Sequence Maturation Screening. Next, we performed randomization of the regions identified as being permissive to mutation. In the first round of sequence optimization, we mutated bases in the outer region of loop #2 or stem and loop #3, highlighted in yellow and orange, respectively, in Figure 4a. Combinations of 2, 3, 4, or 9 nucleotide substitutions were permitted per mutant. This process generated a library of 60,000 sequences that were screened on the microarray for binding to 300 uM cortisol. A total of 24 mutants were identified with a similar or better response to cortisol than the CSS.3 parent sequence. We then combined the functional mutations identified in loop #2 and stem and loop #3 and performed a second round of sequence optimization. A total of 2,000 additional mutants were generated and screened on the microarray against cortisol (0−1 mM, half log dilutions) and DHEAs. From this second round of screening, we identified mutants with improved sensitivity to cortisol while maintaining binding specificity against DHEAs. In Figure 4b we show dose response curves for a selected mutant (Mutant1) along with the CSS.3 parent and a scramble sequence to demonstrate positive and negative dose−responses for cortisol. None of these sequences showed measurable probe dissociation in the presence of DHEAs. Additionally, we were able to assess binding specificity for all sequences on the array against a panel of structurally similar counter targets (including 300 uM DHEAs, progesterone, serotonin, dopamine, estradiol, and 11-deoxycortisol; structures shown in Supporting Information S7). We found that all cortisol binding sequences (including the original CSS.3 parent sequence) showed a strong response to both cortisol and 11-deoxycortisol (an immediate metabolite of cortisol with a very short half-life), a weak response to progesterone, and little to no binding to the remainder of the molecules tested, including DHEAs, estradiol, serotonin, and dopamine. Specificity data for Mutant1 is shown in Figure 4c. The 12 mutants showing the strongest cortisol binding affinity were downselected for further characterization using BLI, as a single strand, without the use of a strand displacement assay. We highlight here the results for Mutant 1 with roughly 3-fold improvement in binding affinity for cortisol compared to the CSS.3 stem-optimized variant (K_D in sISF was 330 nM vs 990 nM for CSS.3_cut3; Figure 4d). A direct comparison of BLI dose response for CSS.3 and Mutant1, along with a diagram of a single stranded BLI assay, is shown in Supporting Information S8. It is observed that the LoD in the BLI instrument for Mutant 1 is significantly better than CSS.3 (Figure S9). This mutant also showed roughly 100-fold selectivity for cortisol over progesterone, which was increased compared to both the full-length CSS.3 aptamer and stem-optimized CSS.3_cut3 (~30-fold each). We also show how the mutant performs in a real biofluid to highlight the translatability of these findings to real-world sensing environments. Because of the difficulties in collecting sufficient volumes of ISF, we used filtered human serum (treated with a 30 kDa molecular weight cutoff (MWCO) filter). Again, the selected mutant maintained roughly 3-fold better binding affinity than the stem-optimized CSS.3_cut3 (Figure 4d).

CONCLUSIONS

Here we demonstrate an approach to aptamer optimization that uses structural characterization data at the molecular level (NMR) to identify unique sequence motifs that are critical to aptamer structure and binding. This information was used to guide rational design of an aptamer truncation with robust conformational switching capability in the presence of target. Additionally, use of the microarray platform allowed us to rapidly study the effect on binding of every possible point mutation in the aptamer sequence, identify regions permissive to mutation, and screen combinations of mutations, resulting in the identification of a cortisol-selective mutant with 3-fold improvement in cortisol binding affinity in just two rounds of microarray screening. Importantly, we were able to perform all screening in a biologically relevant buffer (sISF) and showed direct translation to a human biofluid (filtered human serum). While this work focused on optimization of a cortisol binding aptamer, we have been able to apply the same approach to aptamers for different targets. We believe the approach is broadly applicable for the development of SSAs and that this capability will accelerate aptamer sequence optimization to support the development of rapid, continuous, and wearable biosensing applications.

ASSOCIATED CONTENT

Supporting Information

The Supporting Information is available free of charge at https://pubs.acs.org/doi/10.1021/acssensors.3c02004.

Buffer components, aptamer sequences, NMR spectra, molecular structures, and results for additional targets (PDF)

AUTHOR INFORMATION

Corresponding Author

Jorge L. Chávez − *711th Human Performance Wing, Air Force Research Laboratory, WPAFB, Ohio 45433, United States;* orcid.org/0000-0002-0771-6947; Email: Jorge.Chavez_Benavides.2@us.af.mil

Authors

Monica Wolfe − *711th Human Performance Wing, Air Force Research Laboratory, WPAFB, Ohio 45433, United States; UES, Inc., Dayton, Ohio 45433, United States;* orcid.org/0000-0002-0506-6768

https://doi.org/10.1021/acssensors.3c02004
ACS Sens. 2024, 9, 717−725

Alyssa Cramer − *711th Human Performance Wing, Air Force Research Laboratory, WPAFB, Ohio 45433, United States; UES, Inc., Dayton, Ohio 45433, United States;* orcid.org/0000-0003-2997-5066
Sean Webb − *711th Human Performance Wing, Air Force Research Laboratory, WPAFB, Ohio 45433, United States; UES, Inc., Dayton, Ohio 45433, United States*
Eva Goorskey − *711th Human Performance Wing, Air Force Research Laboratory, WPAFB, Ohio 45433, United States*
Yaroslav Chushak − *711th Human Performance Wing, Air Force Research Laboratory, WPAFB, Ohio 45433, United States; Henry M. Jackson Foundation for the Advancement of Military Medicine, WPAFB, Ohio 45433, United States*
Peter Mirau − *Materials and Manufacturing Directorate, Air Force Research Laboratory, WPAFB, Ohio 45433, United States;* orcid.org/0000-0002-5210-4990
Netzahualcóyotl Arroyo-Currás − *Department of Pharmacology and Molecular Sciences, Johns Hopkins University School of Medicine, Baltimore, Maryland 21205, United States;* orcid.org/0000-0002-2740-6276

Complete contact information is available at: https://pubs.acs.org/10.1021/acssensors.3c02004

Author Contributions

The manuscript was written and edited through contributions from all authors. P.M. and S.W. carried out all NMR experiments. M.W. performed and analyzed all microarray experiments. Y.C. designed and carried out computational modeling experiments. A.C., S.W., and E.G. performed all BLI experiments. M.W., A.C., S.W., P.M., and Y.C. contributed to data generation and manuscript writing and editing. N.A.-C. and J.L.C. were involved in planning, discussion, editing and supervision of the project. All authors have given approval to the final version of the manuscript.

Notes

The views and opinions presented herein are those of the authors and do not necessarily represent the views of the U.S. Department of Defense or its Components.
The authors declare no competing financial interest.

■ ACKNOWLEDGMENTS

Funding was provided by the AFRL 711th Human Performance Wing and the Nano-Bio Materials Consortium (NBMC). E.G. performed this work supported by the Wright Scholars Program. Material is approved for public release. Case Number: AFRL-2023-3920, cleared 09 Aug 2023.

■ ABBREVIATIONS

BLI = biolayer interferometry
BSA = bovine serum albumin
EAB = electrochemical aptamer-based sensor
ISF = interstitial fluid
kDa = kilodalton
MWCO = molecular weight cutoff
NMR = nuclear magnetic resonance
SELEX = systematic evolution of ligands by exponential enrichment
SD = standard deviation
sISF = simulated interstitial fluid
ssDNA = single-stranded DNA
SSA = structure-switching aptamer

■ REFERENCES

(1) Feagin, T. A.; Maganzini, N.; Soh, H. T. Strategies for Creating Structure-Switching Aptamers. *ACS Sensors* **2018**, *3*, 1611−1615.
(2) Wilson, B. D.; Hariri, A. A.; Thompson, I. A. P.; Eisenstein, M.; Soh, H. T. Independent control of the thermodynamic and kinetic properties of aptamer switches. *Nat. Commun.* **2019**, *101* (10), 1−9.
(3) Nutiu, R.; Li, Y. Structure-switching signaling aptamers. *J. Am. Chem. Soc.* **2003**, *125*, 4771−4778.
(4) Ma, X.; Qioa, S.; Sun, H.; Su, R.; Sun, C.; Zhang. Development of structure-switching aptamers for kanamycin detection based on fluorescence resonance energy transfer. *Front. Chem.* **2019**, *7*, 29.
(5) Tang, Z.; Mallikaratchy, P.; Yang, R.; Kim, Y.; Zhu, Z.; Wang, H.; Tan, W. Aptamer Switch Probe Based on Intramolecular Displacement. *J. Am. Chem. Soc.* **2008**, *130*, 11268−11269.
(6) Chen, J.; Fang, Z.; Liu, J.; Zeng, L. A simple and rapid biosensor for ochratoxin A based on a structure-switching signaling aptamer. *Food Control* **2012**, *25*, 555−560.
(7) Morse, D. P. Direct selection of RNA beacon aptamers. *Biochem. Biophys. Res. Commun.* **2007**, *359*, 94−101.
(8) Schoukroun-Barnes, L. R.; Macazo, F. C.; Gutierrez, B.; Lottermoser, J.; Liu, J.; White, R. J. Reagentless, Structure-Switching, Electrochemical Aptamer-Based Sensors. *Annu. Rev. Anal. Chem.* **2016**, *9*, 163−181.
(9) Yoshikawa, A. M.; Rangel, A. E.; Zheng, L.; Wan, L.; Hein, L. A.; Hariri, A. A.; Eisenstein, M.; Soh, H. T. A massively parallel screening platform for converting aptamers into molecular switches. *Nat. Commun.* **2023**, *14*, 2336 DOI: 10.1038/s41467-023-38105-4.
(10) Lam, S. Y.; Lau, H. L.; Kwok, C. K. Capture-SELEX: Selection Strategy, Aptamer Identification, and Biosensing Application. *Biosensors* **2022**, *12*, 1142 DOI: 10.3390/bios12121142.
(11) Lyu, C.; Khan, I. M.; Wang, Z. Capture-SELEX for aptamer selection: A short review. *Talanta* **2021**, *229*, No. 122274.
(12) Yang, K. A.; Pei, R.; Stojanovic, M. N. In vitro selection and amplification protocols for isolation of aptameric sensors for small molecules. *Methods* **2016**, *106*, 58−65.
(13) Parlak, O. Portable and wearable real-time stress monitoring: A critical review. *Sensors and Actuators Reports* **2021**, *3*, No. 100036.
(14) Wang, X.; Walt, D. R. Simultaneous detection of small molecules, proteins and microRNAs using single molecule arrays. *Chem. Sci.* **2020**, *11*, 7896−7903.
(15) Jones, C.; Gwenin, C. Cortisol level dysregulation and its prevalence—Is it nature's alarm clock? *Physiol. Rep.* **2021**, *8*, No. e14644, DOI: 10.14814/phy2.14644.
(16) Torrente-Rodríguez, R. M.; Tu, J.; Yang, Y.; Min, J.; Wang, M.; Song, Y.; Yu, Y.; Xu, C.; Ye, C.; IsHak, W. W.; Gao, W. Investigation of Cortisol Dynamics in Human Sweat Using a Graphene-Based Wireless mHealth System. *Matter* **2020**, *2*, 921−937.
(17) Venugopal, M.; Arya, S. K.; Chornokur, G.; Bhansali, S. A Realtime and Continuous Assessment of Cortisol in ISF Using Electrochemical Impedance Spectroscopy. *Sens. Actuators. A. Phys.* **2011**, *172*, 154.
(18) Laudat, M. H.; Cerdas, S.; Fournier, C.; Guiban, D.; guilhaume, B.; Luton, J. P. Salivary Cortisol Measurement: A Practical Approach to Assess Pituitary-Adrenal Function. *J. Clin. Endocrinol. Metab.* **1988**, *66*, 343−348.
(19) El-Farhan, N.; Rees, D. A.; Evans, C. Measuring cortisol in serum, urine and saliva − are our assays good enough? *Ann. Clin. Biochem.* **2017**, *54*, 308−322.
(20) Gebhart, S.; Faupel, M.; Fowler, R.; Kapsner, C.; Lincoln, D.; McGee, V.; Pasqua, J.; Steed, L.; Wangsness, M.; Xu, F.; Vanstory, M. Glucose Sensing in Transdermal Body Fluid Collected Under Continuous Vacuum Pressure Via Micropores in the Stratum Corneum. *Diabetes Technol. Ther.* **2003**, *5*, 159−166.
(21) Wu, Y.; Tehrani, F.; Teymourian, H.; Mack, J.; Shaver, A.; Reynoso, M.; Kavner, J.; Huang, N.; Furmidge, A.; Duvvuri, A.; Nie, Y.; Laffel, L. M.; Doyle, F. J.; Patti, M. E.; Dassau, E.; Wang, J.; Arroyo-Currás, N. Microneedle Aptamer-Based Sensors for Continuous, Real-Time Therapeutic Drug Monitoring. *Anal. Chem.* **2022**, *94*, 8335 DOI: 10.1021/acs.analchem.2c00829.

(22) Lin, S.; Cheng, X.; Zhu, J.; Wang, B.; Jelinek, D.; Zhao, Y.; Wu, T. Y.; Horrillo, A.; Tan, J.; Yeung, J.; Yan, W.; Forman, S.; Coller, H. A.; Milla, C.; Emaminejad, S. Wearable microneedle-based electrochemical aptamer biosensing for precision dosing of drugs with narrow therapeutic windows. *Sci. Adv.* **2022**, *8*, 4539.
(23) Yi, K.; Wang, Y.; Shi, K.; Chi, J.; Lyu, J.; Zhao, Y. Aptamer-decorated porous microneedles arrays for extraction and detection of skin interstitial fluid biomarkers. *Biosens. Bioelectron.* **2021**, *190*, No. 113404.
(24) Hwang, T. L.; Shaka, A. J. Water Suppression That Works. Excitation Sculpting Using Arbitrary Wave-Forms and Pulsed-Field Gradients. *J. Magn. Reson. Ser. A* **1995**, *112*, 275−279.
(25) Cavanagh, J., Fairbrother, W. J., Palmer, A. G., Rance, M., Skelton, N. J. *Protein NMR Spectroscopy: Principles and Practice*. Protein NMR Spectrosc. Princ. Pract. Academic press **2006** *1*−*915*.
(26) UNAFold Web server. at < http://www.unafold.org/mfold/applications/dna-folding-form.php>.
(27) Cheng, C. Y.; Chou, F. C.; Das, R. Modeling Complex RNA Tertiary Folds with Rosetta. *Methods Enzymol.* **2015**, *553*, 35−64.
(28) Cheatham, T. E.; Case, D. A. Twenty-five years of nucleic acid simulations. *Biopolymers* **2013**, *99*, 969−977.
(29) Schneidman-Duhovny, D.; Inbar, Y.; Nussinov, R.; Wolfson, H. J. PatchDock and SymmDock: servers for rigid and symmetric docking. *Nucleic Acids Res.* **2005**, *33*, W363.
(30) Pettersen, E. F.; Goddard, T. D.; Huang, C. C.; Couch, G. S.; Greenblatt, D. M.; Meng, E. C.; Ferrin, T. E. UCSF Chimera–a visualization system for exploratory research and analysis. *J. Comput. Chem.* **2004**, *25*, 1605−1612.
(31) Yang, K. A.; Chun, H.; Zhang, Y.; Pecic, S.; Nakatsuka, N.; Andrews, A. M.; Worgall, T. S.; Stojanovic, M. N. High-Affinity Nucleic-Acid-Based Receptors for Steroids. *ACS Chem. Biol.* **2017**, *12*, 3103−3112.
(32) Niu, C.; Ding, Y.; Zhang, C.; Liu, J. Comparing two cortisol aptamers for label-free fluorescent and colorimetric biosensors. *Sens. Diagn* **2022**, *1*, 541.
(33) Churcher, Z. R., Johnson, P. E., Johnson, P. *NMR for non-experts; a practical guide for applying NMR methods in studies of aptamer-ligand interactions*. Aptamers (2020) *4*, 3−9.
(34) Sakamoto, T.; *NMR study of aptamers* Aptamers 2017 *1* 13 18
(35) Lam, S. L.; Chi, L. M. Use of Chemical Shifts for Structural Studies of Nucleic Acids. *Prog. Nucl. Magn. Reson. Spectrosc.* **2010**, *56* (3), 289−310.
(36) Li, Y.; Zon, G.; Wilson, W. D. NMR and Molecular Modeling Evidence for a G.A Mismatch Base Pair in a Purine-Rich DNA Duplex. *Proc. Natl. Acad. Sci. U.S.A.* **1991**, *88* (1), 26−30.
(37) Greene, K. L.; Jones, R. L.; Li, Y.; Robinson, H.; Wang, A. H.-J.; Zon, G.; Wilson, W. D. Solution Structure of a GA Mismatch DNA Sequence, d(CCATGAATGG)2, Determined by 2D NMR and Structural Refinement Methods. *Biochemistry.* **1994**, *33* (5), 1053−1062.
(38) Singh, N. K.; Chung, S.; Chang, A. Y.; Wang, J.; Hall, D. A. A non-invasive wearable stress patch for real-time cortisol monitoring using a pseudoknot-assisted aptamer. *Biosens. Bioelectron.* **2023**, *227*, No. 115097.
(39) Catherine, A. T.; Shishido, S. N.; Robbins-Welty, G. A.; Diegelman-Parente, A. Rational design of a structure-switching DNA aptamer for potassium ions. *FEBS Open Bio* **2014**, *4*, 788−795.
(40) Schoukroun-Barnes, L. R.; White, R. J. Rationally Designing Aptamer Sequences with Reduced Affinity for Controlled Sensor Performance. *Sensors* **2015**, *15*, 7754−7767.
(41) Neves, M. A. D.; Shoara, A. A.; Reinstein, O.; Abbasi Borhani, O.; Martin, T. R.; Johnson, P. E. E Optimizing Stem Length to Improve Ligand Selectivity in a Structure-Switching Cocaine-Binding Aptamer. *ACS Sens.* **2017**, *2*, 1539−1545.
(42) Kaur, H.; Yung, L. Y. L.; Addison, C. L. Probing High Affinity Sequences of DNA Aptamer against VEGF165. *PLoS One* **2012**, *7*, 31196.
(43) Heilkenbrinker, A.; Reinemann, C.; Stoltenburg, R.; Walter, J. G.; Jochums, A.; Stahl, F.; Zimmermann, S.; Strehlitz, B.; Scheper, T. Scheper Identification of the target binding site of ethanolamine-binding aptamers and its exploitation for ethanolamine detection. *Anal. Chem.* **2015**, *87*, 677−685.
(44) Wan, L.; Yoshikawa, A.; Eisenstein, M.; Soh, H. T. High-Throughput Strategy for Enhancing Aptamer Performance across Different Environmental Conditions. *ACS Sens.* **2023**, *8*, 2519 DOI: 10.1021/acssensors.2c02106.